FERMILAB-PUB-12-064-T

Annu. Rev. Nucl. Part. Sci. 2012 62 1056-8700/97/0610-00

Twenty-first Century Lattice Gauge Theory: Results from the QCD Lagrangian

Andreas S. Kronfeld
Theoretical Physics Department, Fermi National Accelerator Laboratory, P.O. Box 500, Batavia, Illinois 60510–5100, USA
Email: ask@fnal.gov

Key Words hadron spectrum, chiral symmetry breaking, standard-model parameters, nucleon properties, dark matter, phase transitions

Abstract Quantum chromodynamics (QCD) reduces the strong interactions, in all their variety, to an elegant nonabelian gauge theory. It clearly and elegantly explains hadrons at short distances, which has led to its universal acceptance. Since its advent, however, many of its long-distance, emergent properties have been *believed* to be true, without having been *demonstrated* to be true. This paper reviews a variety of results in this regime that have been established with lattice gauge theory, directly from the QCD Lagrangian. This body of work sheds light on the origin of hadron masses, its interplay with dynamical symmetry breaking, as well as on other intriguing features such as the phase structure of QCD. In addition, nonperturbative QCD is quantitatively important to many aspects of particle physics (especially the quark flavor sector), nuclear physics, and astrophysics. This review also surveys some of the most interesting connections to those subjects.

CONTENTS

Operated by Fermi Research Alliance, LLC under Contract No. De-AC02-07CH11359 with the United States Department of Energy.

1 Introduction

Quantum chromodynamics (QCD) is the modern theory of the strong nuclear force. It is part of the Standard Model of elementary particles and the underpinning of terrestrial and astronomical nuclear physics

The conception of QCD is rightly hailed as a triumph of reductionism, melding the quark model, the idea of color, and the parton model into a dynamical quantum field theory. At the same time, the scope of QCD is rich in emergent phenomena. Symmetries emerge in idealized limits: C, P, and T are exact when the total "vacuum angle" $\bar{\theta} = 0$; chiral symmetries emerge when two or more quark masses vanish (1, 2); and heavy-quark symmetries are revealed as a quark mass goes to infinity (3, 4). More remarkable still are the phenomena that emerge at a dynamically generated energy scale $\Lambda_{\rm QCD}$, the "typical scale of QCD." Much of what is "known" about QCD in this nonperturbative regime has been, for a long time, based on belief. Evidence from high-energy scattering fostered the opinion that QCD explains the strong interactions and, therefore, the belief that QCD exhibits certain properties: otherwise it would not be consistent with lower-energy observations. These emergent phenomena—such as chiral symmetry breaking, the generation of hadron masses much larger than the quark masses, and the thermodynamic phase structure—are the most profound phenomena of gauge theories. The major aim of this review is to survey how lattice QCD has enabled us to replace belief with knowledge. To do so, we shall cover results that are interesting in their own right, influential in a wider arena, qualitatively noteworthy, and/or quantitatively impressive.

The rest of this review is organized as follows. Section 2 introduces the QCD Lagrangian and discusses how, in a general setting, to fix its free parameters. Section 3 gives a short review of lattice-QCD methodology. Hadron masses and their connection to chiral symmetry are discussed in Sections 4 and 5. An output of these calculations are the quark masses and the gauge coupling, which are discussed in Section 6, along with some timely results pertaining to flavor physics. Some interesting properties of nucleons are presented in Section 7. The phase structure of QCD is discussed in Section 8. Section 9 offers some perspective. Appendix A contains pointers to resources for readers who wish to start research in numerical lattice gauge theory.

2 Quantum Chromodynamics

The (renormalized) Lagrangian of QCD has "$1 + n_f + 1$" free parameters:

$$\mathcal{L}_{\rm QCD} = \frac{1}{2g^2}\,\mathrm{tr}[F_{\mu\nu}F^{\mu\nu}] - \sum_{f=1}^{n_f}\bar{\psi}_f(\not{D} + m_f)\psi_f + \frac{i\bar{\theta}}{32\pi^2}\varepsilon^{\mu\nu\rho\sigma}\,\mathrm{tr}[F_{\mu\nu}F_{\rho\sigma}], \qquad (1)$$

where $F^{\mu\nu}$ is the gluon's field strength, $\not{D} = \gamma_\mu(\partial^\mu + A^\mu)$, and ψ_f denotes the quark field of flavor f. The first parameter is the gauge coupling g^2, the next n_f are the quark masses m_f, and the last, $\bar{\theta}$, multiplies an interaction that violates CP symmetry. Experiments have demonstrated the existence of $n_f = 6$ quarks. At energies below the top, bottom, and charm thresholds, however, it is convenient and customary to absorb the short-distance effects of these quarks into a shift of g^2 and then take QCD with $n_f = 5$, 4, or 3. The coupling g^2 diminishes

gradually with increasing energy, stemming from virtual processes of gluons and the n_f active quarks; this "running" is called asymptotic freedom (5, 6).

In the Standard Model, quark masses arise from the matrix of Yukawa couplings to the Higgs field. This matrix can be brought into a form with real eigenvalues $\sqrt{2}m_f/v$ and an overall phase, $\arg\det m$. (Here $v = 246$ GeV is the Higgs field's vacuum expectation value.) In this context, the coupling multiplying $\varepsilon^{\mu\nu\rho\sigma}\,\mathrm{tr}[F_{\mu\nu}F_{\rho\sigma}]$ is altered: $\bar{\theta} = \theta - \arg\det m$, where θ is allowed in QCD as soon as CP violation is admitted. Only the difference $\bar{\theta}$ is observable.

Before saying that a mathematical theory describes or explains the natural world, one must fix its free parameters with the corresponding number of measurements, in this case $1 + n_f + 1$. Because the color of quarks and gluons is confined, the free parameters of QCD must be connected to properties of QCD's eigenstates, which are the color-singlet hadrons. From this perspective, the parameters of QCD may be fixed as follows. The electric-dipole moment of the neutron is too small to measure, leading to a bound $\bar{\theta} < 10^{-11}$. Such delicate cancellation of θ and $\arg\det m$ is a mystery, known as the strong CP problem (7). For QCD calculations it simply means we can set $\bar{\theta} = 0$ with no significant consequences. The rest are tuned to reproduce $1 + n_f$ specific hadronic properties. Because the gauge coupling runs, the physical interpretation of g^2 is predicated on the energy at which it reaches a fiducial value, say $g^2 = 1$. But the mathematics is, strictly speaking, dimensionless, so the energy at which $g^2 = 1$ can be computed only relative to some other standard mass. In practice, it is sensible to choose this standard mass to be insensitive to the quark masses. Finally, the n_f quark masses are best related to n_f hadron masses that depend sensitively on them; for example, the kaon mass is used to tune the strange-quark mass, because $M_K^2 \propto m_s$. With lattice gauge theory (8) one has a tool to relate the QCD Lagrangian directly to such hadronic properties and, thus, fix the parameters this way. It is worth noting, however, that hadronic properties *always* fix the parameters of QCD; the top-quark mass, for example, is measured at the Tevatron via the total energy of the hadrons in jets.

3 Numerical Lattice QCD

Lattice gauge theory (8) was invented in an attempt to understand asymptotic freedom without gauge-fixing and ghosts (9). The key innovation is to formulate nonabelian gauge invariance on a spacetime lattice. Then the functional integrals defining QCD correlation functions are well-defined:

$$\langle \bullet \rangle = \frac{1}{Z} \int \mathcal{D}A\mathcal{D}\psi\mathcal{D}\bar{\psi}\,[\bullet] \exp\left(-S\right), \tag{2}$$

because the measures $\mathcal{D}U$, $\mathcal{D}\psi$, and $\mathcal{D}\bar{\psi}$ are products of a countable number of individual differentials. Here $S = \int d^4x \mathcal{L}_{\mathrm{QCD}}$ is the action, $\bullet$ is just about anything, and Z ensures $\langle 1 \rangle = 1$. This formulation is formally equivalent to classical statistical mechanics, enabling theorists to apply a larger tool-kit to quantum field theory. For example, Wilson used a strong-coupling expansion to lowest order in $1/g^2$ to demonstrate confinement (8).

The results presented below have been obtained by integrating expressions of the form (2) on big computers with Monte Carlo methods. Lattice gauge theory defines QCD mathematically and, thus, in principle provides an algorithm for computing anything. Nevertheless, the computer imposes practical constraints.

To compute anything within a human lifetime, the integrals are defined at imaginary time, $t = -ix_4$, turning Feynman's phase factor into the exponential of Equation 2. A computer, obviously, has finite memory and processing power, so the spatial volume and time extent of the lattice must be finite.

These limitations do not impair the computation of many important classes of quantities. The imaginary time imposes no problem whatsoever for static quantities. The finite volume introduces errors in one-particle states that are exponentially suppressed and, hence, a minor source of uncertainty. In two-particle states, the finite-volume effects are stronger, *but* the volume dependence yields information such as scattering lengths. Similarly, effects of the finite time extent are exponentially suppressed, except in thermodynamics, where it becomes a tool. Finally, the continuum limit must be taken as part of the renormalization procedure (10, 11).

From Equation 2, it is straightforward to derive some simple results for correlation functions. The two-point function

$$\langle \pi(x_4)\pi^\dagger(0)\rangle = \sum_n |\langle 0|\hat{\pi}|\pi_n\rangle|^2 e^{-m_{\pi_n} x_4}, \tag{3}$$

where π is a composite field of definite quantum numbers (e.g., of the pion), and the sum ranges over all radial excitations. For time separation x_4 large enough, a fit to an exponential yields the lowest-lying m_{π_1} and $|\langle 0|\hat{\pi}|\pi_1\rangle|$. Using a larger set of operators, one can extend this method to compute excited-state properties. For a transition with no hadrons in the final state, as in leptonic decays, simply replace $\pi(x_4)$ with a current J:

$$\langle J(x_4)\pi^\dagger(0)\rangle = \sum_n \langle 0|\hat{J}|\pi_n\rangle\langle \pi_n|\hat{\pi}^\dagger|0\rangle e^{-m_{\pi_n} x_4}, \tag{4}$$

in which the only new information is $\langle 0|\hat{J}|\pi_n\rangle$, yielding for large x_4 the decay matrix element of the lowest-lying state. For a transition with one hadron in the final state, one needs a three-point function:

$$\langle \pi(x_4)J(y_4)B^\dagger(0)\rangle = \sum_{mn} \langle 0|\hat{\pi}|\pi_m\rangle\langle \pi_n|\hat{J}|B_m\rangle\langle B_m|\hat{B}^\dagger|0\rangle e^{-m_{\pi_n}(x_4-y_4)-m_{B_m} y_4} \tag{5}$$

in which the only new information is $\langle \pi_n|\hat{J}|B_m\rangle$, yielding for large x_4, y_4 the matrix element between the lowest-lying states. We compute matrix elements for flavor-changing processes, dark-matter detection, and nucleon structure this way.

Equations (3)–(5) are derived by inserting complete sets of eigenstates of the QCD Hamiltonian. The only assumption is that these eigenstates are hadrons. Thus, every successful fit of these formulae for hadronic correlators provides *a posteriori* incremental evidence that hadrons are indeed the eigenstates of QCD.

In all cases of interest, the fermion action is of the form $\bar{\psi}\mathfrak{M}\psi$, where the spacetime matrix $\mathfrak{M}$ is a discretization of the Dirac operator (plus quark mass). Then the fermionic integration in Equation 2 can be carried out by hand:

$$\langle \bullet \rangle = \frac{1}{Z}\int \mathcal{D}A\,[\bullet']\,\det\mathfrak{M}\exp\left(-S_{\text{gauge}}\right), \tag{6}$$

in which the fermionic integration replaces $\psi_i\bar{\psi}_j$ with $[\mathfrak{M}^{-1}]_{ij}$ to yield $\bullet'$. Importance sampling, which is crucial, is feasible only if $\det\mathfrak{M}\exp\left(-S_{\text{gauge}}\right)$ is positive.

Table 1: Pattern of chiral symmetry breaking for n_f lattice fermion fields.

Formulation	flavor×spacetime ⊂ continuum limit
Staggered (14, 15)	$\mathrm{U}(1)^{n_f} \times \Gamma_4 \ltimes \mathrm{SW}_4 \subset \mathrm{SU}(4n_f) \times \mathrm{SU}(4n_f) \times \mathrm{SO}(4)$
Rooted (16)	$\mathrm{U}(1)^{n_f} \times \Gamma_4 \times \mathrm{SW}_4 \subset \mathrm{SU}(n_f) \times \mathrm{SU}(n_f) \times \mathrm{SO}(4)$
Wilson (17)	$\mathrm{SU_V}(n_f) \times \mathrm{SW}_4 \subset \mathrm{SU}(n_f) \times \mathrm{SU}(n_f) \times \mathrm{SO}(4)$
Chiral (18)	$\mathrm{SU}(n_f) \times \mathrm{SU}(n_f) \times \mathrm{SW}_4 \subset \mathrm{SU}(n_f) \times \mathrm{SU}(n_f) \times \mathrm{SO}(4)$

In most cases, a notable exception being the case of nonzero baryon chemical potential, this condition holds.

The determinant $\det \mathfrak{M}$ represents virtual quark-antiquark pairs, also called sea quarks. The matrix inverse $\mathfrak{M}^{-1}$ is the propagator of a valence quark moving through a stew of gluons A and sea quarks. Several quark propagators are sewn together to form hadronic correlation functions, which via Equations 3–5 yield masses and transition matrix elements. The sea $\det \mathfrak{M}$ poses the biggest, and the propagator $\mathfrak{M}^{-1}$ the second biggest, computational challenge. The numerical algorithms become even more demanding as the quark mass is reduced. Lattice-QCD data with unphysically heavy up and down quarks can be extrapolated to the physical limit guided by chiral perturbation theory (12, 13). This step removes the cloud of unphysically massive pions and replaces it with a better (and improvable) approximation to the physical pion cloud.

Because $\det \mathfrak{M}$ and $\mathfrak{M}^{-1}$ are so CPU-intensive, several formulations of lattice fermions are used. As one might anticipate, the computationally fastest and theoretically cleanest methods are not the same. (If one formulation were both fastest and cleanest, no one would use anything else.) Each formulation can be characterized by the amount of flavor symmetry retained by the lattice, as shown in Table 1. Staggered fermions are computationally the fastest, but the flavor group comes in a semi-direct product with the symmetry group of the hypercube, SW_4, and the total number of species in the continuum limit, for n_f fields, is $4n_f$. This fermion doubling is not a problem for the propagators $\mathfrak{M}^{-1}_{\mathrm{stag}}$. For the sea, however, one must take (16) $[\det \mathfrak{M}_{\mathrm{stag}}]^{1/4}$ and appeal to numerical and perturbative evidence that the rooting yields a local field theory in the continuum limit (19).

Because of the expense of sea quarks, many lattice-QCD calculations have been carried out with 2 or fewer (light) flavors. The error entailed in omitting the strange-quark sea is difficult to estimate, so this review mostly considers results with 2+1 flavors in the sea. Here "2+1" denotes the strange sea and two more flavors, for up and down, taken as light as possible. Such simulations made a breakthrough early in the century (20). Now the first results including the charm-quark sea, "2+1+1," are becoming available.

4 Hadron Spectrum

We compute the masses of hadrons not only for a quantitative comparison of QCD with nature, but also to learn how gauge theories generate mass. As we shall see in Section 6, hadron masses are much larger than the sum of the masses of the underlying quarks. The positive binding energy stems from the confining properties of the gluon field and from the kinetic energy of the quarks.

Let us begin with the energy in a flux tube between a static quark and anti-

quark, as a function of separation $\boldsymbol{r}$. The lowest energy level of the flux tube is the potential energy $V(r)$, and the excitations of the flux tube are informative too. The states are labeled $\Sigma_{g,u}, \Pi_{g,u}, \Delta_{g,u}, \ldots$, according to the eigenvalues of gluonic angular momentum along $\boldsymbol{r}$ and of CP [in the subscript g (u) for "(un)gerade," which is German for even (odd)]. The Σ states also carry a superscript $\pm$ denoting the change of sign (or not) of the wave function upon reflection in the plane containing $\boldsymbol{r}$; otherwise such reflections relate degenerate pairs.

Figure 1 shows the lowest-lying levels in the SU(3) gauge theory without light quarks (21). At short distances, the level spacing and ordering is consistent with asymptotic freedom: $V(r)$, for example, is Coulombic up to logarithmic corrections. As r increases, the spacing changes, and at a separation of around 2 fm, the level ordering rearranges to that of a string. The level spacing does not become fully string-like until larger separations (22). The behavior of the excitations is instructive, because the lowest level, $V(r)$, becomes consistent with a string at a relatively short distance around $\frac{1}{2}$ fm (23). A vivid picture of the flux tube has it narrowing as r increases, owing to the attraction between gluons, but the details suggest that the flux tube looks more like a sausage than a string.

One can imagine connecting the ends of the sausage to obtain non-$q\bar{q}$ states called glueballs. Such mesons have no counterpart in the quark model, and lattice gauge theory provides the best (theoretical) evidence that these states do indeed exist. Glueball masses with 2+1 flavors of sea quarks show little change (24) from earlier calculations with no sea quarks (25). In particular, the masses remain consistent with the idea, motivated by lattice QCD, that the $f_J(1710)$ is the lightest scalar glueball (26). The pseudoscalar, tensor, and first radially excited scalar glueballs are all 800–900 MeV higher than the lowest scalar (24).

Lattice QCD has been used to verify the mass spectrum of quark-model hadrons

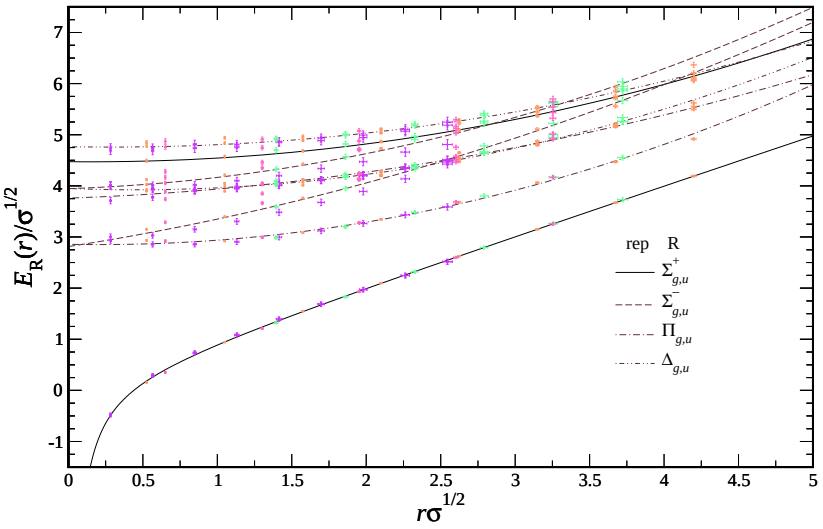

Figure 1: Excitations of the chromoelectric field between two static sources at separation $\boldsymbol{r}$, in units of the string tension $\sigma \approx$ 400–440 MeV. The lowest excitation $E_{\Sigma_g^+}(r) = V(r)$ is the heavy-quark potential, exhibiting Coulombic behavior at short distances and linearly confining behavior at large distances. The higher excitations also exhibit the level ordering of electrodynamics at short distances but the level ordering of a string at large distances. Data from Reference (21).

within a few percent. Figure 2 shows three broad efforts on the spectrum of the isopsin-1 light mesons and the isospin-$\frac{1}{2}$ and -$\frac{3}{2}$ baryons (27, 28, 29, 30). These simulations all include $2 + 1$ flavors of sea quarks, and the error bars, for the most part, are based on thorough analyses of systematics. A satisfying feature of Figure 2 is that the results do not depend in a systematic way on the fermion formulation chosen for the quarks. Even the latest results for the difficult η-η' splitting are encouraging (31, 32, 33).

Figure 2 includes predictions for mesons with quark content $\bar{b}c$ (37, 35, 38). The prediction for the pseudoscalar B_c has been (subsequently) confirmed by experiment (39), whereas the prediction for the vector B_c^* awaits confirmation. These predictions build on successful calculations of the $b\bar{b}$ and $c\bar{c}$ spectra (36, 40, 41, 42, 43) (not shown), which reproduce experiment well.

The most striking aspect of the spectrum is how well it agrees with nature. The nucleons provide almost all the mass in everyday objects, and their masses have been verified within 3.5%. Their mass mostly comes, via $m = E/c^2$, from the kinetic energy of the quarks and the energy stored in the sausage-like flux tube(s) holding the quarks together.

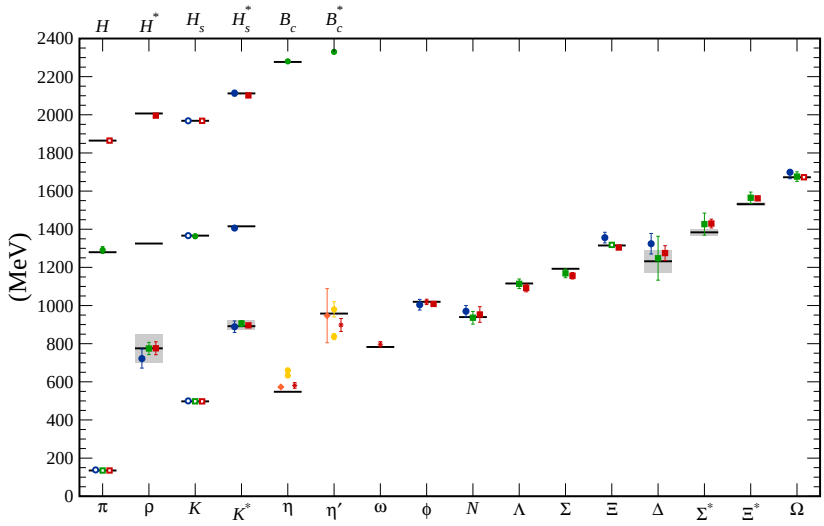

Figure 2: Hadron spectrum from lattice QCD. Comprehensive results for mesons and baryons are from MILC (27, 28), PACS-CS (29), and BMW (30). Results for the η and η' from RBC/UKQCD (31), Hadron Spectrum (32) (also the onlyω mass), and UKQCD (33). Results for heavy-light hadrons from Fermilab-MILC (34), HPQCD (35), and Mohler and Woloshyn (36). Symbol code: circles, squares, and diamonds for staggered, Wilson, and chiral sea quarks; asterisks for anisotropic lattices; open symbols denote masses used to fix parameters; filled symbols (and asterisks) are results. Color code: red, orange, yellow, green, and blue for increasing numbers of ensembles (i.e., lattice spacing and sea-quark mass). Horizontal bars (gray boxes) denote experimentally measured masses (widths). b-flavored mesons offset by -4000 MeV.

5 Chiral Symmetry Breaking

A striking feature of the hadron spectrum in Figure 2 is that the pion has a small mass, around 135 MeV, when the other hadrons have masses more than five times larger. To understand the origin of the difference, Nambu (1) applied lessons from superconductivity, noting (four years before quarks were proposed) that a spontaneously broken axial symmetry would constrain the pion's mass to vanish, with small explicit symmetry breaking allowing it to be nonzero.

If the up and down quarks may be neglected, the QCD Lagrangian acquires an $\mathrm{SU_L}(2) \times \mathrm{SU_R}(2)$ symmetry, thereby explaining the origin of Nambu's axial symmetry. The consequences of spontaneous symmetry breaking were studied further by Goldstone (44), leading to a formula (45),

$$m_\pi^2 \langle \bar{\psi}\psi \rangle = 0, \tag{7}$$

when applied to QCD with massless up and down quarks. The flavor-singlet expectation value $\langle \bar{\psi}\psi \rangle$ is called the chiral condensate. If either factor on the left-hand side of Equation 7 is nonzero, the other must vanish.

From the earliest days of QCD, most physicists were confident that it explained the richness of the strong interactions. Because QCD and Nambu's picture of the pion were both considered right, it was believed that QCD *must* generate a chiral condensate. Until recently, however, no *ab initio* calculation of $\langle \bar{\psi}\psi \rangle$ tested Equation 7. Lattice QCD has now filled this gap (46, 47, 48):

$$\langle \bar{\psi}\psi \rangle = [234 \pm 4 \pm 17 \text{ MeV}]^3 \quad (\overline{\text{MS}} \text{ scheme at 2 GeV}), \tag{8}$$

where the first uncertainty is statistical and the second a combination of systematics, and the quark masses have been adjusted to Nambu's idealization, $m_\mathrm{u} = m_\mathrm{d} \to 0$, m_s physical (48). In summary, QCD's symmetries and dynamics have now been demonstrated to account for the hierarchy between the pion and the other hadron masses.

6 Standard Model Parameters

The Standard Model (with nonzero neutrino masses and mixing angles) has 28 free parameters:

- Gauge couplings: $\boldsymbol{\alpha_\mathrm{s}}$, α_QED, $\alpha_\mathrm{W} = (M_\mathrm{W}/v)^2/\pi$;
- Quark sector: $\boldsymbol{m_\mathrm{u} e^{i\bar{\theta}}}$, $\boldsymbol{m_\mathrm{d}}$, $\boldsymbol{m_\mathrm{s}}$, $\boldsymbol{m_\mathrm{c}}$, $\boldsymbol{m_\mathrm{b}}$, m_t; $\boldsymbol{|V_{us}|}$, $\boldsymbol{|V_{cb}|}$, $\boldsymbol{|V_{ub}|}$, $\boldsymbol{\delta_{KM}}$;
- Lepton sector: m_{ν_1}, m_{ν_2}, m_{ν_3}, m_e, m_μ, m_τ; θ_{12}, θ_{23}, θ_{13}, δ_PMNS, α_{21}, α_{31};
- Standard electroweak symmetry breaking: $v = 246$ GeV, $\lambda = (M_H/v)^2/2$.

Lattice QCD is essential or important in determining the values of eleven parameters (those set in **bold**). Lattice field theory (without QCD) is also useful for shedding light on the Higgs self-coupling λ (49) and the top Yukawa coupling $\sqrt{2}m_\mathrm{t}/v$ (50).

6.1 Quark masses and $\boldsymbol{\alpha_\mathrm{s}}$

Confinement precludes the direct measurement of quark masses. Instead, the masses in Equation 1 must be determined from measurable properties of hadrons.

Table 2: Quark masses from lattice QCD converted to the $\overline{\rm MS}$ scheme and run to the scale indicated. Entries in MeV.

Flavor (scale)	Ref. (28)	Ref. (51)	Ref. (52)	Ref. (53)	Ref. (54)
$\bar{m}_{\rm u}(2\ {\rm GeV})$	1.9 ± 0.2	2.01 ± 0.14	2.37 ± 0.26	2.15 ± 0.11	
$\bar{m}_{\rm d}(2\ {\rm GeV})$	4.6 ± 0.3	4.79 ± 0.16	4.52 ± 0.30	4.79 ± 0.14	
$\bar{m}_{\rm s}(2\ {\rm GeV})$	88 ± 5	92.4 ± 1.5	97.7 ± 6.0	95.5 ± 1.9	
$\bar{m}_{\rm c}(3\ {\rm GeV})$					986 ± 10
$\bar{m}_{\rm b}(10\ {\rm GeV})$					3617 ± 25

The n_f bare quark masses are adjusted until n_f hadron masses of suitable flavor agree with experiment. Four sets of results are shown in Table 2, after being converted to the conventional $\overline{\rm MS}$ scheme. The results in the first, third, and fourth columns are completely independent, employing different formulations for sea quarks and different treatments of electromagnetic effects. The results in the second column are derived from mass ratios [$2m_{\rm s}/(m_{\rm d} + m_{\rm u}) = 27.3 \pm 0.3$ and $m_{\rm u}/m_{\rm d} = 0.42 \pm 0.04$] underlying those in the first column, combined with precise values of the ratio $m_{\rm c}/m_{\rm s} = 11.85 \pm 0.16$ (51) and $\bar{m}_c$ (55).

These results are remarkable for at least two reasons. First, the up and down masses are very small, about four and nine times the electron mass. Quark masses arise from interactions with the Higgs field (or something like it). This sector is, thus, not the origin of much mass. Second, $m_{\rm u}$, though very small, is also very significantly far from zero. This is interesting, because were $m_{\rm u} = 0$, then the additional symmetry of the Lagrangian would render $\bar{\theta}$ unphysical, obviating the strong CP problem (7). (A subtlety could arise from a nonperturbative additive correction to $m_{\rm u}$, but it is probably too small to alter this conclusion.)

The heavy charm- and bottom-quark masses can be determined along the same lines, but the most accurate results come from computing quarkonium correlation functions and taking their continuum limit (56). These functions give spacelike information on the same function measured in the timelike region in $e^+e^- \to c\bar{c}\,(b\bar{b})$. Perturbation theory to order $\alpha_{\rm s}^3$ (57) can then be used to extract the heavy-quark masses and $\alpha_{\rm s}$ (55). This approach yields the results in the fifth column of Table 2, which are in near perfect agreement with the corresponding determinations from e^+e^- collisions (58).

Lattice QCD provides excellent ways to determine the gauge coupling $\alpha_{\rm s} = g^2/4\pi$. In lattice gauge theory, the bare coupling g_0^2 is an input. Alas, for many lattice gauge actions, perturbation theory in g_0^2 converges poorly (59), obstructing a perturbative conversion to the $\overline{\rm MS}$ or other such schemes. Two other strategies are adopted to circumvent this obstacle. One is to compute a short-distance lattice quantity—like a Wilson loop—and reexpress perturbation theory for the Monte Carlo results in a way that eliminates g_0^2 in favor of a renormalized g^2 (59, 60). The other is to compute a short-distance quantity with a continuum limit, and then apply continuum perturbation theory. The quarkonium correlator used for $m_{\rm c}$ and $m_{\rm b}$ is an example (57). Other examples include the Schrödinger functional (61) and the Adler function (62).

Results from several complementary lattice-QCD methods (55,63,64,65,66) are collected in Table 3 and compared to an average of determinations from high-energy scattering and decays (67). One sees excellent consistency among results not only with different discretizations of the determinant for sea quarks, but also when the charmed sea is included (66). An important source of uncertainty is

Table 3: Values of $\alpha_{\rm s}(M_Z)$ from lattice QCD and an average of determinations from high-energy scattering and decays. An update to the values on the first two rows can be found in Reference (54). The central values and error bars from References (64, 65) have been symmetrized to ease comparison. In principle, "nature's sea" includes non-SM colored particles.

$\alpha_{\rm s}(M_Z)$	Observable	Sea formulation	Ref.
0.1174 ± 0.0012	Charmonium correlator	2+1 asqtad staggered	(55)
0.1183 ± 0.0008	Small Wilson loops	2+1 asqtad staggered	(63)
0.1197 ± 0.0013	Schrödinger functional	2+1 improved Wilson	(64)
0.1185 ± 0.0009	Adler function	2+1 overlap	(65)
0.1200 ± 0.0014	Ghost-gluon vertex	2+1+1 twisted Wilson	(66)
0.1186 ± 0.0011	Scattering, τ decay, etc.	nature's sea	(67)

the truncation of perturbation theory, including strategies for matching to the $\overline{\rm MS}$ scheme, and running to scale M_Z. In the example of the small Wilson loops, an independent analysis of the data from Reference (63) has been carried out, yielding $\alpha_{\rm s}(M_Z) = 0.1192 \pm 0.011$ (68), to be compared with the second line of Table 3.

The agreement of the lattice- and perturbative QCD results for $\alpha_{\rm s}$, $m_{\rm c}$, and $m_{\rm b}$ is especially compelling since QCD is the union of the quark model of hadrons and the parton model of high-energy scattering. The consistency is evidence that the QCD of hadrons and the QCD of partons are the same.

6.2 Flavor Physics

As mentioned in Section 2, the quark masses arise from the electroweak interactions. In a basis where the mass matrix is diagonal, the W boson couples to all combinations of $(u, c, t, \ldots) \otimes (d, s, b, \ldots)^{\rm T}$ quarks. Along with the SU(2) gauge coupling, the udW vertex carries a factor V_{ud}, and similarly for all other combinations. As a change of basis (from the W to the mass basis), the Cabibbo-Kobayashi-Maskawa (69, 70) (CKM) quark-mixing matrix V is unitary. After considering global symmetries of the gauge interactions, one sees that the CKM matrix has fewer parameters than a generic unitary matrix. For three generations, three mixing angles and one CP-violating phase remain, and a convenient choice consists of $|V_{us}|$, $|V_{ub}|$, $|V_{cb}|$, and $\arg V_{ub}^*$.

Lattice QCD calculations play a key role in flavor physics. The phase and, except for $|V_{tb}|$, all magnitudes of the CKM matrix can be accessed via processes for which the corresponding lattice-QCD calculations are under good control:

$$V = \begin{pmatrix} |V_{ud}| & |V_{us}| & |V_{ub}| & \arg V_{ub}^* \\ \pi \to \ell\nu & K \to \ell\nu & B \to \tau\nu & \langle K^0|\bar{K}^0\rangle \\ n \to p e^- \bar{\nu} & K \to \pi\ell\nu & B \to \pi\ell\nu & \\ |V_{cd}| & |V_{cs}| & |V_{cb}| & \\ D \to \ell\nu & D_s \to \ell\nu & B \to D\ell\nu & \\ D \to \pi\ell\nu & D \to K\ell\nu & B \to D^*\ell\nu & \\ |V_{td}| & |V_{ts}| & |V_{tb}| & \\ \langle B_d|\bar{B}_d\rangle & \langle B_s|\bar{B}_s\rangle & (\text{no } t\bar{q} \text{ hadrons}) & \end{pmatrix}. \qquad (9)$$

These leptonic and semileptonic decays (first two rows) or meson-antimeson os-

cillations (phase and third row) have one hadron in the initial state and one (or none) in the final state. Thus, all of these flavor-changing amplitudes can be computed in lattice QCD via Equations 4 or 5. Semileptonic transition form factors for $K \to \pi\ell\nu$ (71,72), $B \to \pi\ell\nu$ (73,74), and $B \to D^*\ell\nu$ (75) are sensitive to the mixing angles, and K^0-$\bar{K}^0$ mixing (76,77,78,79) is sensitive to the CP-violating phase. Together with calculations of D-meson decays (80,81,82) and $B^0_{(s)}$-$\bar{B}^0_{(s)}$ mixing (83), the full suite of lattice-QCD calculations overdetermines the CKM matrix and, thus, tests for consistency. The semileptonic D decays are considered crosschecks. Taking $|V_{cd}|$ and $|V_{cs}|$ from CKM unitarity (which is very precise), one finds that lattice-QCD calculations of the kinematic distributions (80) and the normalization of the rate (81,82) agree with several experiments.

Non-SM particles could spoil this picture, which is why it is interesting to test it in detail. With a fourth generation of quarks and leptons, the 3×3 submatrix generically would not be unitary. If other particles, such as supersymmetric partners of the known particles, change quark flavor, the SM relation between a flavor-changing process and V is spoiled. The off-diagonal elements are small—$|V_{us}| \sim 0.2$, $|V_{cb}| \sim 4 \times 10^{-2}$, and $|V_{ub}| \sim 3 \times 10^{-3}$—so it is not out of the question that (widely anticipated) TeV-scale particles make detectable contributions.

During the first decade of the 21st century, all simple, pertinent lattice-QCD calculations were carried out with 2+1 sea quarks. In most cases, more than one collaboration has published results, and, in many cases, the literature covers more than one fermion formulation for the quarks. The calculations most directly connected to determining the CKM parameters have been combined—with an eye to correlations in the errors—in Reference (84).

Despite the broad agreement of flavor-physics measurements with the Standard Model, some tension appears in global fits to the four CKM parameters (85). Some mild discrepancies also arise in a few isolated processes, and here we shall consider two leptonic decays where lattice-QCD plays a key role.

Let us begin by noting that the semileptonic and leptonic determinations of $|V_{us}|$ are completely compatible (86) [based on References (87,88,89) and (71,72)]. The vector component of the W boson mediates the former, and the axial current the latter. Since they are compatible, nothing other than the SM W boson is needed to describe these decays.

The present status of semileptonic and leptonic determinations of $|V_{ub}|$ is not so tidy. Combining lattice QCD for the $B \to \pi\ell\nu$ form factor (73, 74) with measurements from BaBar (90) yields $|V_{ub}| = (2.95 \pm 0.31) \times 10^{-3}$; with Belle (91) $|V_{ub}| = (3.43 \pm 0.33) \times 10^{-3}$. The average taken here is $|V_{ub}|_{B\to\pi\ell\nu} = (3.19 \pm 0.32) \times 10^{-3}$. Combining lattice QCD for the B-meson decay constant (83, 92) with the world average of the rate for $B^+ \to \tau^+\nu$ (93), however, suggests $|V_{ub}|_{B\to\tau\nu} = (4.95 \pm 0.55) \times 10^{-3}$, which deviates by 2.8σ from $|V_{ub}|_{B\to\tau\nu}$. This discrepancy could be explained if another particle (or particles) were to mediate the decays with a coupling different from the W boson's $V - A$. Examples include a charged Higgs boson (94,95) or a right-handed vector current (96). The plot thickens when one considers inclusive charmless semileptonic B decays, which are mediated by all possible currents. These decays imply a value of $|V_{ub}|$ in between those from the two exclusive methods.

A cautionary tale comes, however, from $D_s \to \mu^+\nu$, and $D_s \to \tau^+\nu$ decays. In 2008, the measured branching fractions exceeded the SM prediction by nearly 4σ, as shown in Figure 3. This discrepancy relies on the decay constant f_{D_s}

from lattice QCD (97, 87). Using the same methods as for the π and K decay constants (87,98), the D_s decay constant can be computed to 1–2%. At the time, some experimenters asserted that either the lattice-QCD calculations were wrong or that new physics mediated the decay. For example, the excesses of $D_s \to \ell^+\nu$ could be due to leptoquarks (99), with a few-percent amplitude constructively interfering. As more measurements came in, however, the discrepancy softened, and it is now only 1.6σ. Although the lattice-QCD average has increased 8 MeV, the experimental average has decreased 18 MeV. The early measurements fluctuated up; perhaps the same holds for $B \to \tau\nu$.

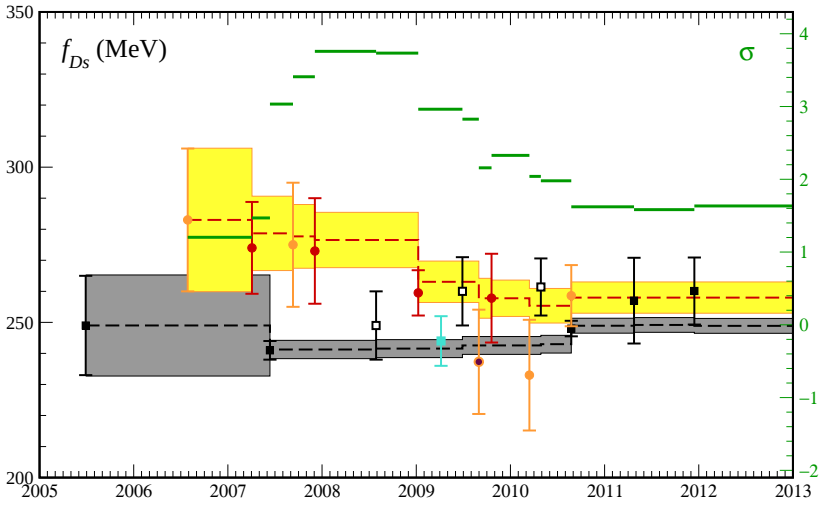

Figure 3: Comparison of f_{D_s} since 2005. The green line (right axis) shows the discrepancy in σ. The gray band shows the running average of 2+1-flavor lattice QCD calculations from Fermilab-MILC (97, 92), HPQCD (87, 98), and PACS-CS (100). [The 2-flavor cyan point from ETM (101) is not included in the average.] The yellow band shows the running average of measurements from BaBar, Belle, and CLEO-*c* (93). Updated from Reference (102).

7 Nucleon Matrix Elements, Dark Matter, and the LHC

Two of the most compelling questions facing particle physics are the origin of electroweak symmetry breaking and the composition of dark matter. The experiments built to address them rely on the humble proton and neutron. The Large Hadron Collider (LHC) collides pp—and the Tevatron $p\bar{p}$, and detectors buried deep underground hope to see weakly-interacting massive particles (WIMPs) scatter of the protons and neutrons in nuclei. To interpret the results of these experiments, it is helpful to calculate certain matrix elements of the nucleon (103).

Let us start with WIMP-nucleon scattering. The key information needed to compute the cross section is

$$\sigma_q = m_q \langle N|\bar{q}q|N\rangle = m_q \frac{\partial M_N}{\partial m_q}, \tag{10}$$

for quarks q in the nucleon, including virtual quarks like s and c. The partial derivative should be taken with the other n_f QCD parameters held fixed. Usually

Table 4: Table of scalar-density matrix elements. The first and fourth rows use 2 flavors of sea quarks; the others 2+1. Entries in MeV.

Method	σ_{u+d}	σ_s	Reference
πN scattering $\oplus$ baryon octet masses	45 ± 8	122 ± 143	(104, 106)
	64 ± 7	378 ± 135	(105, 106)
Lattice QCD Feynman-Hellman	$53 \pm 2^{+21}_{-7}$		(108)
Lattice QCD M_N χPT	$47 \pm 8 \pm 3$	$31 \pm 15 \pm 4$	(109)
Lattice QCD Feynman-Hellman		$59 \pm 7 \pm 8$	(110)
Lattice QCD matrix element		$30 \pm 8 \pm 21$	(111)
Lattice QCD Feynman-Hellman	$39 \pm 4^{+18}_{-7}$	$34 \pm 14^{+28}_{-23}$	(112)
Lattice QCD Feynman-Hellman	$31 \pm 3 \pm 4$	$71 \pm 34 \pm 59$	(113)

the light quarks are combined into the isospin-singlet

$$\sigma_{u+d} = \tfrac{1}{2}(m_{\mathrm{u}} + m_{\mathrm{d}})\langle N|(\bar{u}u + \bar{d}d)|N\rangle. \tag{11}$$

(The reader should beware of factors of 2 in the definitions of these and similar quantities, sometimes denoted Σ, in the literature.) For WIMP detection, σ_{u+d} and σ_s are especially important.

Until recent lattice-QCD calculations became available, the light-quark "sigma term" has been extracted from πN scattering, with the help of chiral perturbation theory (104,105). As seen in the first two row of the σ_{u+d} column of Table 4, the extraction depends more on assumptions than on the experimental data. To estimate σ_s, information from the baryon octet masses is used (106). Unfortunately, this information must be subtracted from σ_{u+d}, rendering σ_s rather unstable. It is a pressing need to improve both matrix elements (107).

Equation 10 suggests two methods to compute σ_q in lattice QCD, either from a three-point function, as in Equation 5, or by studying the mass dependence of the nucleon mass M_N. The latter is known as the Feynman-Hellman theorem, and here one can either reweight the Monte Carlo ensemble to take the derivative locally, or study the chiral extrapolation to obtain a global handle on the derivative. Several recent results are compiled in Table 4. From a quantitative perspective, it seems that the results are still settling down, though they tend to favor lower values of σ_{u+d}. More striking (and self-consistent with low σ_{u+d}), the results for σ_s dramatically contradict the high values used in WIMP phenomenology. Thus, even if these results are not yet as mature as those reported in Sections 4, 5, and 6, their influence could be precocious.

In pp or $p\bar{p}$ collisions, the essential long-distance ingredient in computing cross sections are the moments of the parton distribution functions. These moments are given by matrix elements of local operators, similar to the $\bar{q}q$ in Equation 10 but with different Dirac structures, such as γ^μ or $\gamma^\mu\gamma^5$, and derivatives (to pull out higher powers of the momentum fraction). Figure 4 shows some recent lattice-QCD results for the nonsinglet average momentum fraction $\langle x\rangle_{u-d}$ as a function of simulation m_π^2 (114,115,116), compared with two phenomenological results (117, 118). The latter are obtained by fitting experimental data, which exist over a large but limited range of x, to reasonable parametrizations. In principle, the lattice-QCD moments add extra information, but the status of the chiral extrapolation may not be ready for this step, although some functional forms do indeed extrapolate to results (114, 115) that agree with the fits to experiment.

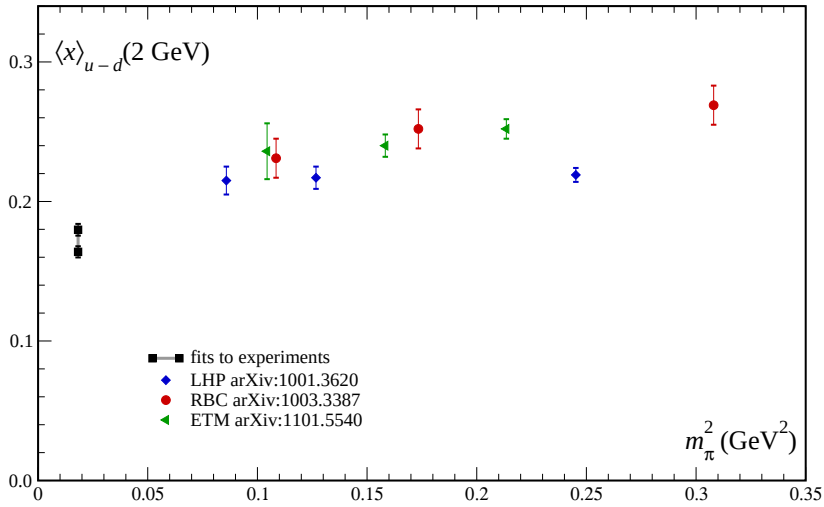

Figure 4: Nonsinglet average momentum fraction $\langle x \rangle_{u-d}$ vs. m_π^2 from LHP (114), RBC and UKQCD (115), and ETM (116). The last has 2+1+1 flavors of sea quark, the others 2+1. Fits to experiment from MSTW (117) and ABM (118); others fall between these two.

Note that earlier work with only 2 flavors of sea quark yielded confusing results. The low moments of quark densities from 2+1- and 2+1+1-flavor simulations are approaching the point where the lattice-QCD results could be incorporated into the traditional fits of experimental data. For collider phenomenology, the real challenge for lattice QCD is to compute similar moments of the gluon density, which are less well constrained by low-energy experiments.

8 QCD Thermodynamics

The previous sections consider isolated hadrons at zero temperature. Soon after the Big Bang, however, the universe was much hotter than it is now, and in neutron stars, for example, the baryon density is much higher than in normal nuclear matter. These phenomena motivate the study of the thermodynamics of QCD. Even within lattice gauge theory, thermodynamics is a vast subject (119, 120), so this review touches only on some of the more fascinating aspects.

Thermodynamics starts with thermal averages in the canonical ensemble

$$\langle \bullet \rangle = \frac{\mathrm{Tr}\left[\bullet\, e^{-\hat{H}/T}\right]}{\mathrm{Tr}\, e^{-\hat{H}/T}}, \tag{12}$$

where T is the temperature, and the traces Tr are over the Hilbert space of the QCD Hamiltonian $\hat{H}$. In fact, the average on the left-hand side of Equation 12 is precisely that of Equation 2; the time extent N_4 specifies the temperature $T = (N_4 a)^{-1}$. The eigenstates of $\hat{H}$—a.k.a. hadrons—do not change with T, but as T increases the vacuum no longer dominates the way it does in Equations 3–5, and multi-hadron states begin to play a role in the thermal average.

The simplest observables are quantities like the energy, pressure, and entropy density, and order parameters sensitive to symmetry breaking. The thermal state can either restore a spontaneously broken symmetry of the vacuum or be a state

of broken symmetry itself. Of course, the (approximate) symmetry of the Hamiltonian remains intact. Figure 5 shows order parameters for deconfinement and chiral symmetry restoration, as the temperature increases from normal hadronic matter to the "quark-gluon plasma." Both quantities change dramatically for a temperature around 145–170 MeV (123, 124), but neither, especially deconfinement, exhibits the sharp change characteristic of a phase transition. Studying a whole suite of thermodynamic observables confirms that the transition is smooth crossover (125, 122). This result came as a surprise, and below we shall see why.

The crossover means that as the early universe cools, hot matter gradually becomes more and more like a gas of distinct hadrons. With a first-order phase transition, on the other hand, bubbles of the hadronic phase would form inside the quark-gluon plasma. Without a real phase transition, the quark-gluon plasma is not necessarily a fluid of quasi-free quarks and gluons. The eigenstates in Equation 12 remain color singlets, but a thermal medium can be qualitatively different. First, thermal fluctuations encompass states with many overlapping hadrons, so color can propagate from one hadron to the next, as if deconfined. Second, the thermal average applies nearly equal Boltzmann weights to states of both parities, so chiral symmetry can be restored in the thermal average, even though the vacuum breaks it.

The nature of the QCD phase transition is influenced by the physical values of the up, down, and strange quark masses. For vanishing quark masses, the transition would be first order, but as the masses are increased, the strength of

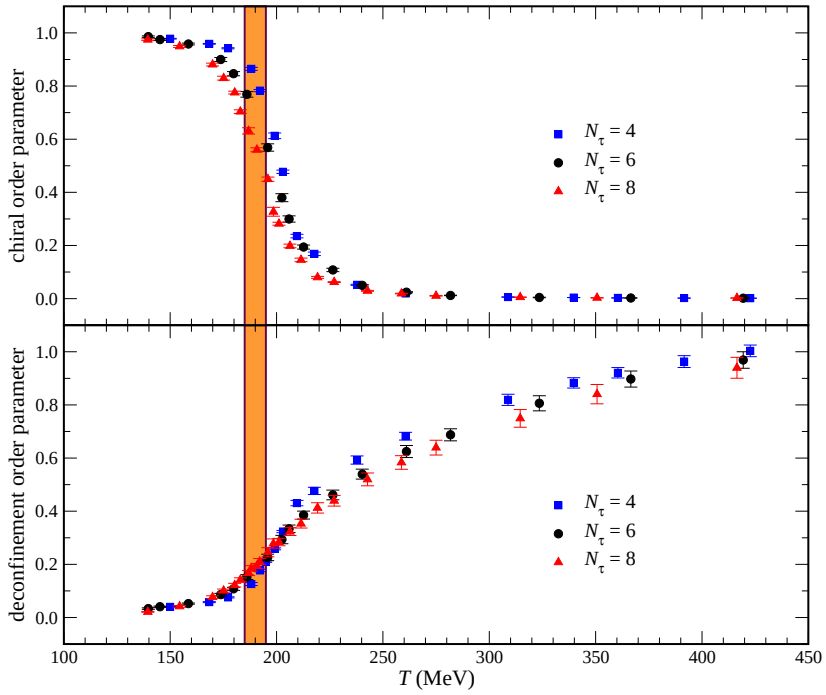

Figure 5: Order parameters for deconfinement (bottom) and chiral symmetry restoration (top), as a function of temperature. The physical temperature $T = a/N_\tau$, where a is the lattice spacing. Agreement for several values of N_τ thus indicates that discretization effects from the lattice are under control. Data from References (121, 122).

the transition diminishes. As sketched in Figure 6a, the physical quark masses (cf. Table 2) are just large enough to render the transition a crossover. If the light quark masses—crucially $m_{\rm s}$—were around half their physical size, the universe would cool through a first-order transition. Before lattice QCD established these results, the conventional wisdom was that the quark masses are somewhat larger than shown in Table 2, yet small enough to remain in the first-order basin of massless quarks.

At nonzero baryon density (chemical potential $\mu \neq 0$), the fermion determinant becomes complex, which is an obstacle to importance sampling. This restricts lattice-QCD calculations to small μ. It is thought that the transition becomes first order for $\mu \sim$ few 100 MeV (126), as shown in Figure 6b, but the matter is not yet settled (127).

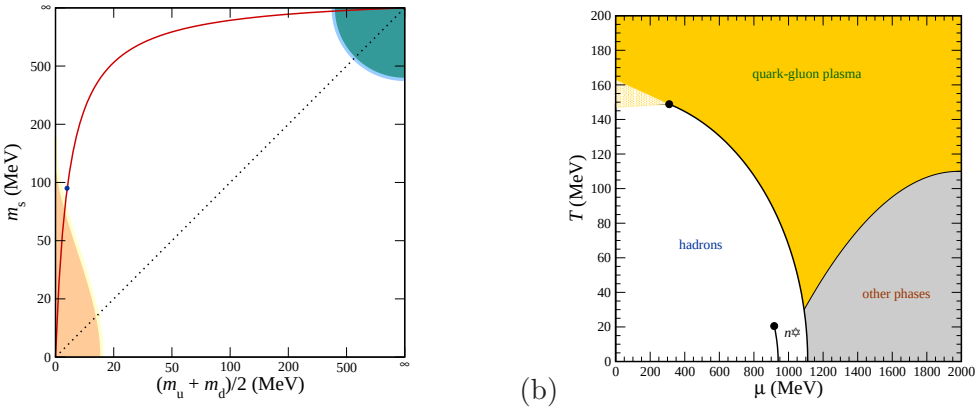

Figure 6: QCD phase diagrams. (a) The $m_{\rm s}$-$\frac{1}{2}(m_{\rm u} + m_{\rm d})$ plane at $(\mu, T) = (0, T_c)$, showing the order of the transition: the shaded regions at very small and nearly infinite masses are first order; the red line shows the physical ratio of $2m_{\rm s}/(m_{\rm u}+m_{\rm d})$. (b) The μ-T plane, showing the crossover at small μ determined from lattice QCD; the neutron star ($n\star$) and "other" phases are expected, but lattice QCD has not yet is a position to provide useful information.

9 Summary and Outlook

The topics discussed above demonstrate that we have learned a great deal in this century about QCD from lattice gauge theory. The 21st century is still young, and the prospects for learning more are bright.

Although the mass spectrum of the lowest-lying hadrons has been well verified, it will be interesting to extend the calculations to excited states (128, 129) and even to small nuclei like the deuteron (130) or the H dibaryon (131,132). Beyond QCD, one can wonder whether nature uses gauge theories to generate quark, lepton, and weak boson masses (133).

Most of the calculations related to flavor physics are entering an industrial phase, where the objective is higher and higher precision. An exception is the measurement of direct CP violation in the kaon system. This calculation requires a two-pion final state, and although the formalism for handling this state has long been available (134), only now have $K \to \pi\pi$ amplitudes become feasible (135, 136). These finite-volume techniques are related to methods (137) for computing scattering lengths (138, 139), with many applications in hadronic physics.

Acknowledgments

The author would like to thank Jimmy Juge, Julius Kuti, Colin Morningstar, Eric Gregory, Craig McNeile, and Frithjof Karsch for supplying data plotted above. Fermilab is operated by Fermi Research Alliance, LLC, under Contract No. DE-AC02-07CH11359 with the U.S. Department of Energy.

A Tools

Research in lattice QCD requires computer time and software. Through several efforts around the world, these needs pose lower obstacles than ever before. Several groups have made documented software available, so that new programs can be modeled after existing code, rather than being built from scratch. Furthermore, many groups make ensembles of lattice gauge fields available, principally via the International Lattice Data Grid (ILDG) (140). In exchange for suitable citation of a paper describing the content of the ensembles, anyone can use these simulation data for their own physics analyses. In many cases, even more ensembles are available from collaborations with newer ensembles under generous terms: most of these collaborations have some core physics analyses but are happy if the expensive simulation data are mined for more results.

The ILDG has portals in Australia (141), continental Europe (142), Japan (143), the United Kingdom (144), and the United States (145). The technical underpinnings are described in Reference (146). Further ensembles are available from the Gauge Connection (147) and the QCDOC Gauge Field Configuration Archive (148).

Publicly available software can be obtained from the USQCD Collaboration (149). Newcomers should start with one of the Applications Packages, CHROMA, CPS, MILC, or FERMIQCD. A useful tutorial on this software has been put together by Joó (150) (slides only).

Two kinds of computing are important to lattice gauge theory, *capability* and *capacity*. One needs access to computers of the greatest capability—i.e., able to run large-memory jobs with huge appetite in CPU time—to generate the ensembles of lattice gauge fields. On these ensembles an analysis consists of a huge number of small-to-medium computing demands; this step requires computers of high capacity. Most university groups have access to computers of sufficiently high capacity to analyze publicly available ensembles.

LITERATURE CITED

1. Nambu Y, Phys. Rev. Lett. 4:380 (1960).
2. Weinberg S, Phys. Rev. Lett. 18:188 (1967).
3. Shifman MA, Voloshin MB, Sov. J. Nucl. Phys. 45:292 (1987).
4. Isgur N, Wise MB, Phys. Lett. B232:113 (1989).
5. Politzer HD, Phys. Rev. Lett. 30:1346 (1973).
6. Gross DJ, Wilczek F, Phys. Rev. Lett. 30:1343 (1973).
7. Kim JE, Carosi G, Rev. Mod. Phys. 82:557 (2010), 0807.3125.
8. Wilson KG, Phys. Rev. D10:2445 (1974).
9. Wilson KG, Nucl. Phys. Proc. Suppl. 140:3 (2005), hep-lat/0412043.
10. Symanzik K, Nucl. Phys. B226:187 (1983).
11. Symanzik K, Nucl. Phys. B226:205 (1983).

12. Sharpe SR, Shoresh N, Phys. Rev. D62:094503 (2000), hep-lat/0006017.
13. Bijnens J, PoS LAT2007:004 (2007), 0708.1377.
14. Susskind L, Phys. Rev. D16:3031 (1977).
15. Sharatchandra HS, Thun HJ, Weisz P, Nucl. Phys. B192:205 (1981).
16. Hamber HW, Marinari E, Parisi G, Rebbi C, Phys. Lett. B124:99 (1983).
17. Wilson KG, Quantum chromodynamics on a lattice, in *New Phenomena in Subnuclear Physics*, Zichichi A, Plenum, New York, 1977.
18. Ginsparg PH, Wilson KG, Phys. Rev. D25:2649 (1982).
19. Donald GC, Davies CTH, Follana E, Kronfeld AS, Phys. Rev. D84:054504 (2011), 1106.2412.
20. HPQCD, MILC, and Fermilab Lattice, Davies CTH, et al., Phys. Rev. Lett. 92:022001 (2004), hep-lat/0304004.
21. Juge KJ, Kuti J, Morningstar C, Phys. Rev. Lett. 90:161601 (2003), hep-lat/0207004.
22. Juge KJ, Kuti J, Morningstar C, QCD string formation and the Casimir energy, in *Confinement 2003*, Suganuma H, et al., pp. 233–248, Singapore, 2004, World Scientific, hep-lat/0401032.
23. Lüscher M, Weisz P, JHEP 0207:049 (2002), hep-lat/0207003.
24. UKQCD, Richards CM, Irving AC, Gregory EB, McNeile C, Phys. Rev. D82:034501 (2010), 1005.2473.
25. Morningstar CJ, Peardon MJ, Phys. Rev. D60:034509 (1999), hep-lat/9901004.
26. Sexton J, Vaccarino A, Weingarten D, Phys. Rev. Lett. 75:4563 (1995), hep-lat/9510022.
27. MILC, Aubin C, et al., Phys. Rev. D70:094505 (2004), hep-lat/0402030.
28. Bazavov A, et al., Rev. Mod. Phys. 82:1349 (2010), 0903.3598.
29. PACS-CS, Aoki S, et al., Phys. Rev. D79:034503 (2009), 0807.1661.
30. BMW, Dürr S, et al., Science 322:1224 (2008), 0906.3599.
31. RBC and UKQCD, Christ NH, et al., Phys. Rev. Lett. 105:241601 (2010), 1002.2999.
32. Hadron Spectrum, Dudek JJ, et al., Phys. Rev. D83:111502 (2011), 1102.4299.
33. UKQCD, Gregory EB, Irving AC, Richards CM, McNeile C, (2011), 1112.4384.
34. Fermilab Lattice and MILC, Bernard C, et al., Phys. Rev. D83:034503 (2011), 1003.1937.
35. HPQCD, Gregory EB, et al., Phys. Rev. D83:014506 (2011), 1010.3848.
36. Mohler D, Woloshyn RM, Phys. Rev. D84:054505 (2011), 1103.5506.
37. HPQCD and Fermilab Lattice, Allison IF, et al., Phys. Rev. Lett. 94:172001 (2005), hep-lat/0411027.
38. HPQCD, Gregory EB, et al., Phys. Rev. Lett. 104:022001 (2010), 0909.4462.
39. CDF, Aaltonen T, et al., Phys. Rev. Lett. 100:182002 (2008), 0712.1506.
40. HPQCD, Gray A, et al., Phys. Rev. D72:094507 (2005), hep-lat/0507013.
41. Meinel S, Phys. Rev. D79:094501 (2009), 0903.3224.
42. Fermilab Lattice and MILC, Burch T, et al., Phys. Rev. D81:034508 (2010), 0912.2701.
43. HPQCD, Dowdall RJ, et al., (2011), 1110.6887.
44. Goldstone J, Nuovo Cim. 19:154 (1961).
45. Goldstone J, Salam A, Weinberg S, Phys. Rev. 127:965 (1962).
46. DeGrand T, Liu Z, Schaefer S, Phys. Rev. D74:094504 (2006), hep-

lat/0608019.
47. JLQCD, Fukaya H, et al., Phys. Rev. Lett. 104:122002 (2010), 0911.5555.
48. JLQCD and TWQCD, Fukaya H, et al., Phys. Rev. D83:074501 (2011), 1012.4052.
49. Gerhold P, Jansen K, JHEP 1004:094 (2010), 1002.4336.
50. Gerhold P, Jansen K, JHEP 0907:025 (2009), 0902.4135.
51. HPQCD, Davies CTH, et al., Phys. Rev. Lett. 104:132003 (2010), 0910.3102.
52. Blum T, et al., Phys. Rev. D82:094508 (2010), 1006.1311.
53. BMW, Dürr S, et al., Phys. Lett. B701:265 (2011), 1011.2403.
54. HPQCD, McNeile C, Davies CTH, Follana E, Hornbostel K, Lepage GP, Phys. Rev. D82:034512 (2010), 1004.4285.
55. HPQCD, Allison I, et al., Phys. Rev. D78:054513 (2008), 0805.2999.
56. Bochkarev A, de Forcrand P, Nucl. Phys. B477:489 (1996), hep-lat/9505025.
57. Chetyrkin KG, Kühn JH, Sturm C, Eur. Phys. J. C48:107 (2006), hep-ph/0604234.
58. Chetyrkin KG, et al., Phys. Rev. D80:074010 (2009), 0907.2110.
59. Lepage GP, Mackenzie PB, Phys. Rev. D48:2250 (1993), hep-lat/9209022.
60. HPQCD, Mason Q, et al., Phys. Rev. Lett. 95:052002 (2005), hep-lat/0503005.
61. Lüscher M, Narayanan R, Weisz P, Wolff U, Nucl. Phys. B384:168 (1992), hep-lat/9207009.
62. Baikov PA, Chetyrkin KG, Kühn JH, Phys. Rev. Lett. 101:012002 (2008), 0801.1821.
63. HPQCD, Davies CTH, et al., Phys. Rev. D78:114507 (2008), 0807.1687.
64. PACS-CS, Aoki S, et al., JHEP 10:053 (2009), 0906.3906.
65. JLQCD, Shintani E, et al., Phys. Rev. D82:074505 (2010), 1002.0371.
66. ETM, Blossier B, et al., (2012), 1201.5770.
67. Bethke S, Eur. Phys. J. C64:689 (2009), 0908.1135.
68. Maltman K, Leinweber D, Moran P, Sternbeck A, Phys. Rev. D78:114504 (2008), 0807.2020.
69. Cabibbo N, Phys. Rev. Lett. 10:531 (1963).
70. Kobayashi M, Maskawa T, Prog. Theor. Phys. 49:652 (1973).
71. ETM, Lubicz V, et al., Phys. Rev. D80:111502 (2009), 0906.4728.
72. RBC and UKQCD, Boyle PA, et al., Eur. Phys. J. C69:159 (2010), 1004.0886.
73. HPQCD, Gulez E, et al., Phys. Rev. D73:074502 (2006), hep-lat/0601021.
74. Fermilab Lattice and MILC, Bailey JA, et al., Phys. Rev. D79:054507 (2009), 0811.3640.
75. Fermilab Lattice and MILC, Bernard C, et al., Phys. Rev. D79:014506 (2009), 0808.2519.
76. Aubin C, Laiho J, Van de Water RS, Phys. Rev. D81:014507 (2010), 0905.3947.
77. RBC and UKQCD, Aoki Y, et al., Phys. Rev. D84:014503 (2011), 1012.4178.
78. BMW, Dürr S, et al., Phys. Lett. B705:477 (2011), 1106.3230.
79. SWME, Bae T, et al., (2011), 1111.5698.
80. Fermilab Lattice, MILC, and HPQCD, Aubin C, et al., Phys. Rev. Lett. 94:011601 (2005), hep-ph/0408306.
81. HPQCD, Na H, Davies CTH, Follana E, Lepage GP, Shigemitsu J, Phys. Rev. D82:114506 (2010), 1008.4562.
82. HPQCD, Na H, et al., Phys. Rev. D84:114505 (2011), 1109.1501.

83. HPQCD, Gámiz E, Davies CTH, Lepage GP, Shigemitsu J, Wingate M, Phys. Rev. D80:014503 (2009), 0902.1815.
84. Laiho J, Lunghi E, Van de Water RS, Phys. Rev. D81:034503 (2010), 0910.2928, with updates at `http://latticeaverages.org/`.
85. Lunghi E, Soni A, Phys. Lett. B666:162 (2008), 0803.4340.
86. Flavianet Lattice Averaging Group, Colangelo G, et al., Eur. Phys. J. C71:1695 (2011), 1011.4408.
87. HPQCD, Follana E, Davies CTH, Lepage GP, Shigemitsu J, Phys. Rev. Lett. 100:062002 (2008), 0706.1726.
88. BMW, Dürr S, et al., Phys. Rev. D81:054507 (2010), 1001.4692.
89. MILC, Bazavov A, et al., PoS LATTICE2010:074 (2010), 1012.0868.
90. BaBar, del Amo Sanchez P, et al., Phys. Rev. D83:032007 (2011), 1005.3288.
91. Belle, Ha H, et al., Phys. Rev. D83:071101 (2011), 1012.0090.
92. Fermilab Lattice and MILC, Bazavov A, et al., (2011), 1112.3051.
93. Heavy Flavor Averaging Group, Asner D, et al., (2010), 1010.1589.
94. Akeroyd AG, Chen CH, Phys. Rev. D75:075004 (2007), hep-ph/0701078.
95. Deschamps O, et al., Phys. Rev. D82:073012 (2010), 0907.5135.
96. Crivellin A, Phys. Rev. D81:031301 (2010), 0907.2461.
97. Fermilab Lattice, MILC, and HPQCD, Aubin C, et al., Phys. Rev. Lett. 95:122002 (2005), hep-lat/0506030.
98. HPQCD, Davies CTH, et al., Phys. Rev. D82:114504 (2010), 1008.4018.
99. Dobrescu BA, Kronfeld AS, Phys. Rev. Lett. 100:241802 (2008), 0803.0512.
100. PACS-CS, Namekawa Y, et al., Phys. Rev. D84:074505 (2011), 1104.4600, complete error budget in journal only.
101. ETM, Blossier B, et al., JHEP 0907:043 (2009), 0904.0954.
102. Kronfeld AS, The f_{D_s} puzzle, in *XXIX Physics in Collision*, Kawagoe K, et al., Tokyo, 2009, Universal Academy Press, 0912.0543.
103. Bhattacharya T, et al., (2011), 1110.6448.
104. Koch R, Z. Phys. C15:161 (1982).
105. Pavan MM, Strakovsky II, Workman RL, Arndt RA, PiN Newslett. 16:110 (2002), hep-ph/0111066.
106. Borasoy B, Meißner UG, Ann. Phys. 254:192 (1997), hep-ph/9607432.
107. Ellis J, Olive KA, Sandick P, New J. Phys. 11:105015 (2009), 0905.0107.
108. JLQCD, Ohki H, et al., Phys. Rev. D78:054502 (2008), 0806.4744.
109. Young RD, Thomas AW, Phys. Rev. D81:014503 (2010), 0901.3310.
110. MILC, Toussaint D, Freeman W, Phys. Rev. Lett. 103:122002 (2009), 0905.2432.
111. JLQCD, Takeda K, et al., Phys. Rev. D83:114506 (2011), 1011.1964.
112. BMW, Dürr S, et al., Phys. Rev. D85:014509 (2012), 1109.4265.
113. QCDSF, Horsley R, et al., Phys. Rev. D85:034506 (2012), 1110.4971.
114. LHP, Bratt JD, et al., Phys. Rev. D82:094502 (2010), 1001.3620.
115. RBC and UKQCD, Aoki Y, et al., Phys. Rev. D82:014501 (2010), 1003.3387.
116. ETM, Dinter S, et al., PoS LATTICE2010:135 (2010), 1101.5540.
117. Martin AD, Stirling WJ, Thorne RS, Watt G, Eur. Phys. J. C63:189 (2009), 0901.0002.
118. Alekhin S, Blümlein J, Moch S, (2012), 1202.2281.
119. DeTar C, Heller UM, Eur. Phys. J. A41:405 (2009), 0905.2949.
120. Fodor Z, Katz SD, The phase diagram of quantum chromodynamics, in *Landolt-Börnstein: Relativistic Heavy-Ion Physics*, Stock R, volume 23, p. 2.2, Springer, Berlin, 2010, 0908.3341.

121. Cheng M, et al., Phys. Rev. D77:014511 (2008), 0710.0354.
122. Bazavov A, et al., Phys. Rev. D80:014504 (2009), 0903.4379.
123. Wuppertal-Budapest, Borsányi S, et al., JHEP 1009:073 (2010), 1005.3508.
124. HotQCD, Bazavov A, et al., (2011), 1111.1710.
125. Aoki Y, Endrődi G, Fodor Z, Katz SD, Szabó KK, Nature 443:675 (2006), hep-lat/0611014.
126. Levkova L, (2012), 1201.1516.
127. de Forcrand P, Philipsen O, JHEP 11:012 (2008), 0808.1096.
128. Hadron Spectrum, Bulava JM, et al., Phys. Rev. D79:034505 (2009), 0901.0027.
129. Hadron Spectrum, Edwards RG, Dudek JJ, Richards DG, Wallace SJ, Phys. Rev. D84:074508 (2011), 1104.5152.
130. NPLQCD, Beane SR, et al., (2011), 1109.2889.
131. NPLQCD, Beane SR, et al., Phys. Rev. Lett. 106:162001 (2011), 1012.3812.
132. HAL QCD, Inoue T, et al., Phys. Rev. Lett. 106:162002 (2011), 1012.5928.
133. Del Debbio L, PoS LATTICE2010:004 (2011), 1102.4066.
134. Lellouch L, Lüscher M, Commun. Math. Phys. 219:31 (2001), hep-lat/0003023.
135. RBC and UKQCD, Blum T, et al., Phys. Rev. D84:114503 (2011), 1106.2714.
136. RBC and UKQCD, Blum T, et al., (2011), 1111.1699.
137. Lüscher M, Nucl. Phys. B354:531 (1991).
138. NPLQCD, Beane SR, et al., Nucl. Phys. A794:62 (2007), hep-lat/0612026.
139. NPLQCD, Torok A, et al., Phys. Rev. D81:074506 (2010), 0907.1913.
140. International Lattice Data Grid (ILDG), `http://www.usqcd.org/ildg/`.
141. ILDG Australia, `http://cssm.sasr.edu.au/ildg/`.
142. ILDG Europe, `http://hpc.desy.de/ldg/`.
143. ILDG Japan, `http://ws.jldg.org/QCDArchive/`.
144. ILDG UK, `http://www.gridpp.ac.uk/qcdgrid/`.
145. ILDG USA, `http://www.usqcd.org/ildg/`.
146. Beckett MG, et al., Comput. Phys. Commun. 182:1208 (2011), 0910.1692.
147. MILC, `http://qcd.nersc.gov/`.
148. RBC and UKQCD, `http://lattices.qcdoc.bnl.gov/`.
149. USQCD Software Committee, `http://www.usqcd.org/usqcd-software/`.
150. Joó B, Numerical exercises in lattice field theory, `http://www.int.washington.edu/talks/WorkShops/int_07_2b/` (2007).